Identifying the Principal Modes of Variation in Human Thoracic Aorta Morphology

Mariano E. Casciaro, Eng,† Damian Craiem, PhD,*†‡§ Gilles Chironi, MD,‡§ Sebastian Graf, PhD,*† Laurent Macron, MD,§‖ Elie Mousseaux, MD,§‖ Alain Simon, MD,‡§ and Ricardo L. Armentano, PhD**

Purpose: Diagnosis and management of thoracic aorta (TA) disease demand the assessment of accurate quantitative information of the aortic anatomy. We investigated the principal modes of variation in aortic 3-dimensional geometry paying particular attention to the curvilinear portion.

Materials and Methods: Images were obtained from extended noncontrast multislice computed tomography scans, originally intended for coronary calcium assessment. The ascending, arch, and descending aortas of 500 asymptomatic patients (57 ± 9 y, 81% male) were segmented using a semiautomated algorithm that sequentially inscribed circles inside the vessel cross-section. Axial planes were used for the descending aorta, whereas oblique reconstructions through a toroid path were required for the arch. Vessel centerline coordinates and the corresponding diameter values were obtained. Twelve size and shape geometric parameters were calculated to perform a principal component analysis.

Results: Statistics revealed that the geometric variability of the TA was successfully explained using 3 factors that account for $\sim$80% of total variability. Averaged aortas were reconstructed varying each factor in 5 intervals. Analyzing the parameter loadings for each principal component, the dominant contributors were interpreted as vessel size (46%), arch unfolding (22%), and arch symmetry (12%). Variables such as age, body size, and risk factors did not substantially modify the correlation coefficients, although some particular differences were observed with sex.

Conclusions: We conclude that vessel size, arch unfolding, and symmetry form the basis for characterizing the variability of TA morphology. The numerical data provided in this study as supplementary material can be exploited to accurately reconstruct the curvilinear shape of normal TAs.

Key Words: principal component analysis, noncontrast multislice computed tomography, 3-dimensional arterial modeling, aortic arch

(*J Thorac Imaging* 2013;00:000–000)

From the *Facultad de Ingeniería, Ciencias Exactas y Naturales (FICEN), Universidad Favaloro; †Consejo Nacional de Investigaciones Cientificas y Técnicas (CONICET), Buenos Aires, Argentina; ‡Centre de Médecine Préventive Cardiovasculaire; ‖Département de Radiologie Cardiovasculaire, Hôpital Européen Georges Pompidou; and §APHP, Paris Descartes University, INSERM U970, Paris, France.

The authors declare no conflicts of interest.

Reprints: Damian Craiem, PhD, Facultad de Ingeniería, Ciencias Exactas y Naturales (FICEN), Universidad Favaloro, Solis 453, CP 1078, Ciudad de Buenos Aires, Argentina (e-mails: dcraiem@favaloro.edu.ar).

Supplemental Digital Content is available for this article. Direct URL citations appear in the printed text and are provided in the HTML and PDF versions of this article on the journal's Website, www.thoracicimaging.com.

Early detection of cardiovascular diseases in a subclinical stage has strengthened efforts to find new noninvasive diagnostic tools. Within several available approaches for risk stratification in asymptomatic adults, multislice computed tomography (MSCT) imaging for coronary calcium assessment was recently recommended in persons at intermediate-risk and even low 10-year-risk levels.[1] The coronary artery calcium (CAC) test exploits the high contrast between calcium and soft tissue and estimates the total amount of calcium within the coronary arteries in a single score at a low radiation dose (typical values are < 2 mSv). Routine CAC tests provide new possibilities to assess extracoronary information. For instance, calcifications are not restricted to coronary arteries, and they can also be found all along the thoracic aorta (TA).[2] Consequently, our group has recently explored the whole TA in a large cohort of patients, extending the scanning field of view (FOV) to include the top of the aortic arch. All this extracoronary information was utilized to build a 3-dimensional (3D) geometric model of the TA and to analyze the effects of aging on the vessel morphology, as described in prior work.[3] Within this process, in which geometric features of the TA curvilinear portion were intensely investigated, we remarked a rich interpatient variability in TA morphology that deserved further attention.[4]

The assessment of TA size is usually used for an early diagnosis of aneurysms or other TA diseases.[5] Furthermore, recent statistics on the incidence and management of TA disease were reported, and the importance of early recognition and diagnosis by modern imaging modalities such as MSCT was enhanced.[6] The combination of MSCT and 3D reconstruction algorithms is essential for endovascular stent design and placement.[7] In a procedure known as endovascular repair of TA, the use of stents originally designed with the shape of the abdominal aorta might limit their success.[8] In particular, these devices often fail to properly adapt to the tortuous shape of the aortic arch and other segments of the TA, inducing changes in blood flow, thrombosis, and/or direct injury to the endothelium.[8,9] There are no commercially available stent grafts for aortic aneurysms of the ascending, root, and arch locations, although investigational designs that include fenestrations to accommodate the branch supra-aortic arteries are being evaluated.[10,11] Further efforts are needed to assess accurate morphologic information of the human TA.[12] Ideally, an anatomic database containing statistical models should be created to explain the natural TA geometric variability using a set of meaningful parameters.

In another context, aortic geometry has proven to be a determinant in primary and secondary blood flow patterns, such as vortex and helix blood flow, verified in numerical

simulations[13] and in vivo.[14] This influence is strongly related to plaque formation in TA, together with the recognized influence of flow-induced shear-stress on atherogenesis.[15,16] Novel quantitative reports, including detailed TA geometric features in 3D for a large cohort of patients, are then indispensable for both the development of innovative stent grafts and the understanding of blood flow patterns.

The aim of this paper was to study the 3D TA morphology in a large cohort of patients and to identify the principal modes of geometric variation. Meaningful geometric variables were selected to perform a principal component analysis (PCA). PCA often requires the placement of landmark points along boundaries to analyze shape variability; however, hybrid parameters can be envisaged as well.[17] In our approach, a set of meaningful size and shape parameters were extracted from TA segmentation and then included into a statistical factor analysis to assess TA geometric variability. The principal factors that explained aortic geometric variations were identified and anatomically interpreted. Animations of the morphologic change associated with each factor and the numerical information to reconstruct the averaged vessels are provided as supplementary material (Videos F1, F2, and F3, Supplemental Digital Contents 1, 2, and 3, http://links.lww.com/JTI/A48, http://links.lww.com/JTI/A49, http://links.lww.com/JTI/A50).

MATERIALS AND METHODS

In the following section, the segmentation algorithm to isolate the TA from noncontrast MSCT images is summarized. Further details can be found in Craiem et al.[3] The subsequent Population Description and Data Acquisition section includes the population description, image acquisition details, and the statistical analysis.

Semiautomatic Segmentation Algorithm

The segmentation process starts when the user places seed points within the ascending and descending aorta at the level of the pulmonary artery, named CA and CD, respectively (Fig. 1A). Using these points, an automatic adaptive circle-fitting algorithm will extract the central skeleton and the circular cross-section of the vessel. The steps of the algorithm that inscribes a circle inside the vessel cross-section area are:

- A median filter within a 10×10 cm region of interest for noise removal.
- A morphologic opening filter using a circular structuring element of radius $r = 1$ cm to separate the aorta from surrounding tissues.
- A binarization isodata algorithm.
- An iterative growth algorithm in which a circle located in the seed expands until it touches the limits of the aorta. Contact with this limit generates the displacement of the center of the circle in the opposite direction to the point of contact, and growth is resumed. The algorithm ends when the biggest circle inscribed inside the vessel cross-section is found.

The result of this algorithm is a point of coordinates (x_i, y_i, z_i) corresponding to the center of the circle and a radius r_i determining the area of the circumference that approximates the cross-section of the aorta in that position (Figs. 1B, C). This algorithm is sequentially applied over the axial CT slices for the descending portion of the aorta below the seed point CD (Fig. 1B) and over oblique planes reconstructed in steps of 2-degree angles by trilinear interpolation following a semitoroidal path joining the CA and CD points, until a maximum angle of 240 degrees is obtained or the coronary sinus is found (Fig. 1C). In both cases, the center point of the circle found at the end of the algorithm is used as a seed point for the next slice or reconstructed plane. The algorithm assumes the aorta as a variable radius cylinder deformed in space along a curve corresponding to its central skeleton. This simplification would ensure that the cross-section of the aorta, perpendicular to its central skeleton is always circular. As the curvilinear portion of the aorta does not necessarily follow a strict toroidal shape[14,18] and the descending aorta might not be perfectly vertical, a postprocessing correction is performed. Accordingly, orthogonal planes to the central skeleton obtained from the previous step are reconstructed, and the circle-fitting algorithm is rerun to find the final aortic diameters for each centerline point. In this correction stage, the new reconstructed planes are perpendicular to the true aortic skeleton thus ensuring a more adequate assessment of the vessel diameter.

The resulting TA model has 2 elements: (i) an ordered set of points for the central skeleton following the aortic path; and (ii) a circular cross-section for each point of the skeleton. This model allows the measurement of geometric and shape parameters of the aorta and can be easily adapted to mesh the aortic surface to perform volumetric or surface calculations.

From the central skeleton of the aorta, a linear regression plane passing through the midpoint between CA and CD (called point "o") is calculated using the orthogonal vectors v1 and v2 shown in Figure 2A. Combining the model with this plane of regression, the following 12 geometric size and shape parameters were measured:

- Mean TA arch diameter (D), including the whole curvilinear portion from CA to CD.
- Total TA length (L) and volume (V).
- Radius of curvature (R) calculated as the inverse of the TA arch curvature from CA to CD.
- Vessel tortuosity (T) calculated as the arc-chord ratio between points CA and CD minus 1.
- Aortic arch width corresponding to the distance between CD and CA (Fig. 2A) and aortic arch height corresponding to the distance between point "o" and point C_{90} (Fig. 2A).
- Distance from center point "o" to 45-degree (C_{45}) and 135-degree (C_{135}) vectors (Fig. 2A).
- Arch symmetry calculated as the difference between C_{135} and C_{45} vectors measured in centimeters.
- The inclination angle α between the plane of regression and the line connecting point "o" with C_{90}. It is an indicator of the arch top inclination (Fig. 2B).
- The transversal angle β between the projection of the lines connecting C_{90} with points CA and CD, over the axial plane (perpendicular to the regression plane). It is an indicator of the inclination of the ascending and descending portions (Fig. 2C).

Population Description and Data Acquisition

We modeled the aorta of 500 asymptomatic patients from the Centre de Médecine Préventive Cardiovasculaire unit of the Georges Pompidou Hospital (Paris, France) studied between September 2009 and October 2010. Subjects were hospitalized in an ongoing cardiovascular risk

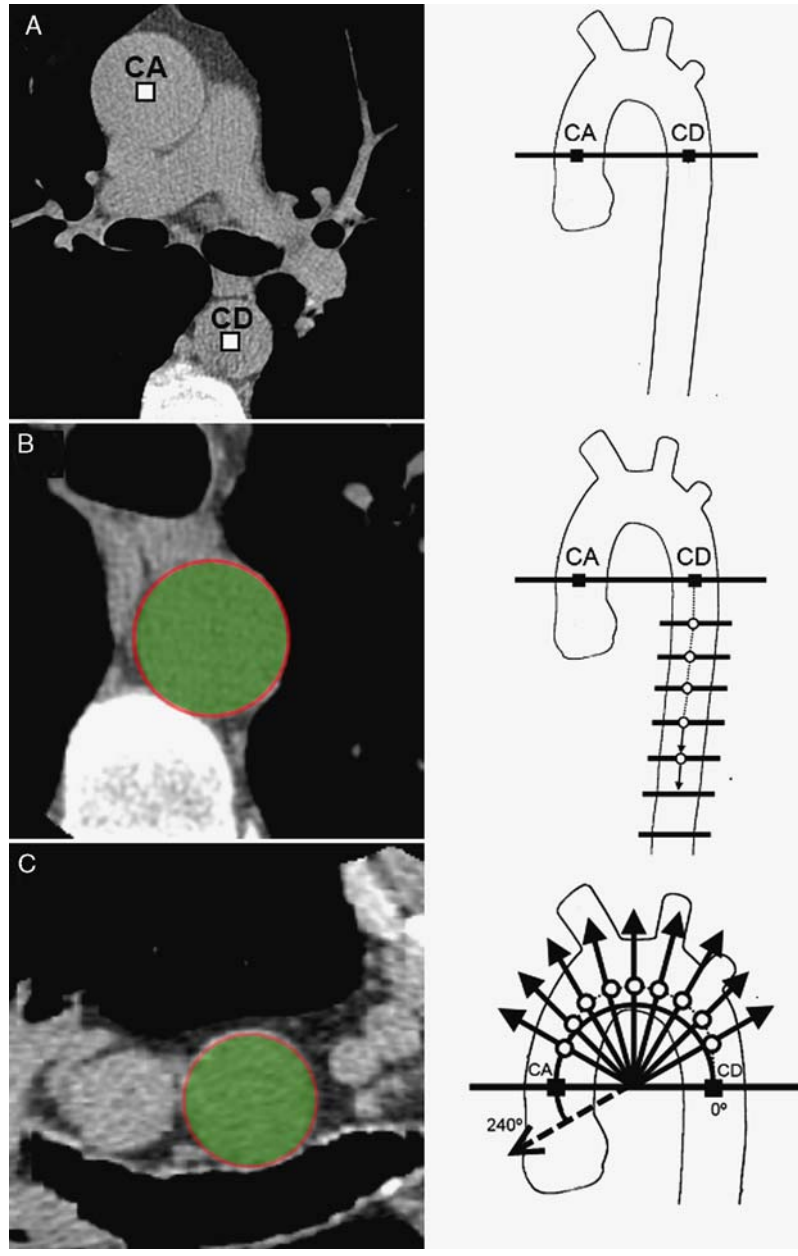

FIGURE 1. A, Axial tomographic slice at the level of pulmonary artery where aortic ascending (CA) and descending (CD) seed points are placed by the user. B, Descending aorta is automatically segmented with an algorithm that finds the inscribed circles (green) inside vessel cross-section in sequential axial slices. C, The same algorithm is applied in reconstructed oblique planes that follow a toroid path to segment the aortic curvilinear portion.

screening program on the basis of cardiovascular risk stratification including Framingham risk score (FRS) calculation,[19] subclinical atherosclerosis imaging,[20] and CAC scoring by thoracic noncontrast CT. Subjects were consecutively selected from the hospital database provided they had undergone complete TA imaging during the CAC measurement. Hypertension was defined by a resting brachial blood pressure of 140 and/or 90 mm Hg or above and/or by the presence of antihypertensive medication. Hypercholesterolemia was defined by a fasting low-density lipoprotein (LDL) cholesterol level of > 3.3 mmol/L or by the presence of LDL-lowering drug treatment. Blood glucose was measured after overnight fast, and diabetes was defined by a fasting blood glucose level of 7 mmol/L or above or by the presence of antidiabetic medication. Past or current smokers were defined as subjects who smoke or had smoked at least 1 cigarette per day, every day or someday. All subjects were free of any history or symptom of cardiovascular disease. This retrospective study was authorized by the Commission Nationale de l'informatique et des Libertés and in accordance with the Declaration of Helsinki. Images were obtained in a single breath-hold (craniocaudal direction from above the aortic arch to the diaphragm) using an MSCT scanner (64-slice Light-speed

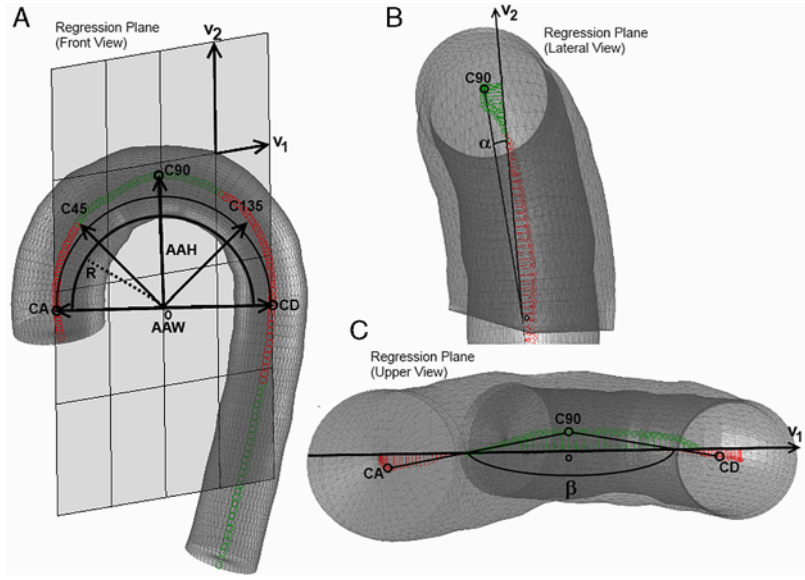

FIGURE 2. A, Aortic mesh and regression plane defined by vectors $\vec{v}_1$ and $\vec{v}_2$. Twelve geometric parameters are calculated to describe the aortic geometry as listed in the Materials and methods section. B, Lateral view of aortic mesh, where the inclination angle α is defined. C, Upper view of aortic mesh, where the transversal angle β is defined. Green and red points indicate TA centerline in front and behind the regression plane, respectively. AAH indicates aortic arch height; AAW, aortic arch width.

VCT; GE Health Care, Milwaukee, WI) with a slice thickness of 2.5 mm, *xy*-resolution of 0.47 mm/pixel, 120 kV, tube current 250 mA, 250 ms exposure, a 2350 mm FOV, and electrocardiogram-triggering at 60% of the RR interval (middiastole).

Statistical Analysis

Baseline characteristics of men and women were compared using a χ^2 statistic for dichotomous variables and analysis of variance for continuous variables. Size and shape parameters were expressed by median and interquartile values (25th and 75th percentile) and compared using a Wilcoxon nonparametric test. Statistical analyses were performed with JMP (SAS, NC) software, and significance was set at $P < 0.05$.

A PCA was performed using a data vector combining the 12 shape and size parameters of each patient.[21] Before the analysis, all variables were normalized by subtracting the mean value and dividing the result by its SD.

The 3 main factors were identified in a PCA scree plot to show the amount of total variance explained by each principal component. Aortic morphology variation, as a function of principal components variation, was studied by plotting an average aorta for patients whose *i*-th principal component F_i fell inside 1 of the following 5 intervals:

$$F_i < -\sqrt{\lambda_i}; -\sqrt{\lambda_i} < F_i < -\frac{\sqrt{\lambda_i}}{2}; -\frac{\sqrt{\lambda_i}}{2} < F_i < \frac{\sqrt{\lambda_i}}{2}; \frac{\sqrt{\lambda_i}}{2} < F_i < \sqrt{\lambda_i}; \sqrt{\lambda_i} < F_i, \quad (1)$$

where λ_i represents the *i*-th eigenvalue of the covariance matrix. For visualization and interpretation purposes, an average aorta was calculated for each interval. This was performed by matching all the corresponding vessels in a unique regression plane and aligning them around the midpoint between CA and CD (point "o"). For every centerline position, an average centerline and diameter value is obtained for all the aligned aortas. The numerical values of the averaged aortic models for the 5 intervals and animations including smooth transitions along these intervals are provided as supplementary material (Videos F1, F2, and F3, Supplemental Digital Contents 1, 2, and 3, http://links.lww.com/JTI/A48, http://links.lww.com/JTI/A49, http://links.lww.com/JTI/A50).

For the first 3 significant eigenvalues ($\lambda_i > 1$) of the covariance matrix, the corresponding eigenvectors were calculated. Using these vectors and the corresponding eigenvalues, the correlation coefficient (r) between the geometric parameters and the principal components were calculated and represented in a parallel plot. Parameters with $r > 0.6$ were considered to be strongly associated with that factor, whereas parameters with $0.4 < r < 0.6$ were considered as mildly associated. Finally, and to further understand the source of TA geometric variability, correlation coefficients were also calculated in 6 subgroups obtained after splitting the whole population in half, separated by median values of (i) age, (ii) FRS, and (iii) body surface area (BSA). The maximum and minimum correlation values in each geometric parameter after division by age, FRS, or BSA were indicated in the parallel plot, together with an individual curve for women in order to visualize the effect of sex.

RESULTS

Population characteristics are detailed in Table 1. Age ranged from 32 to 83 years. Most of the patients had at least 1 risk factor, and the 10-year FRS range was 1% to 32%. Women, representing 19% of the population, were older ($P < 0.001$) and had lower BSA ($P < 0.001$) and lower 10-year FRS ($P < 0.001$) compared with men. The prevalence of traditional risk factors was similar between groups. The percentage of patients receiving treatment for hypertension and hypercholesterolemia was 92% and 68%, respectively. The geometric parameters selected to describe

TABLE 1. Clinical Characteristics of the Study Population

Patients Characteristics	Total	Men	Women
No. subjects [n (%)]	500 (100)	405 (81)	95 (19)
Age (y)	57 ± 9	56 ± 9	61 ± 7*
BSA (m^2)	1.95 ± 0.21	2.0 ± 0.2	1.7 ± 0.2*
10-y Framingham risk (%)	11 ± 6	12 ± 6	5 ± 3*
Hypertension [n (%)]	245 (49)	201 (50)	44 (46)
Hypercholesterolemia [n (%)]	400 (80)	322 (80)	78 (82)
Diabetes [n (%)]	45 (9)	39 (10)	6 (6)
Past or current smoking [n (%)]	279 (56)	235 (58)	44 (46)

Data are mean ± SD or n (%).
*$P < 0.001$ (t test with respect to men).

TA morphology are listed in Table 2. The average TA height and width of the curvilinear portion were 4.7 and 7.8 cm, respectively. The radius of curvature was 3.5 cm. In fact, the curvilinear shape was not strictly symmetrical: the vector C_{135} was slightly longer than vector C_{45}, evidencing a differential deformation in the distal section of the arch, near the proximal descending portion. Vessel centerlines were not completely coplanar with their regression planes (Fig. 2A), as evidenced by mean inclination and transversal angles of 8 and 152 degrees, respectively. Globally, values were in agreement with previous reports.[3,22] In the female population, all size parameters (diameter, length, volume, arch width and height, and C_{45} and C_{135} vectors) were significantly lower ($P < 0.001$) than those in men, whereas shape parameters (tortuosity, arch symmetry, inclination, and transversal angles) did not differ. In addition, the radius of curvature was lower in women than in men ($P < 0.01$).

TABLE 2. TA Morphology

	Median Q1-Q3 (CQV%)		
Size and Shape Parameters	**Total**	**Men**	**Women**
Mean diameter (cm)	2.9 2.8-3.1 (6)	2.9 2.8-3.1 (6)	2.8** 2.7-2.9 (4)
Length (cm)	28.0 26.4-30.0 (6)	28.3 26.5-30.3 (7)	26.9** 25.5-28.3 (6)
Volume (cm^3)	157 132-182 (16)	156 136-187 (16)	137** 119-152 (12)
Radius of curvature (cm)	3.5 3.2-3.9 (9)	3.6 3.3-3.9 (9)	3.4* 3.2-3.7 (8)
Tortuosity	0.81 0.71-0.94 (14)	0.83 0.70-0.93 (14)	0.82 0.72-1.02 (18)
Aortic arch width (cm)	7.8 7.1-8.5 (9)	7.9 7.3-8.6 (8)	7.0** 6.6-7.8 (9)
Aortic arch height (cm)	4.7 4.2-5.1 (9)	4.8 4.3-5.1 (9)	4.3** 4.0-4.6 (8)
C_{45} vector (cm)	4.2 3.9-4.6 (8)	4.3 4.0-4.6 (8)	3.9** 3.6-4.2 (8)
C_{135} vector (cm)	4.4 4.0-4.9 (10)	4.5 4.1-5.0 (10)	4.2** 3.9-4.6 (8)
Arch symmetry ($C_{135}-C_{45}$) (cm)	0.2 −0.1 to 0.6 (160)	0.2 −0.2 to 0.6 (170)	0.3 0.0-0.6 (98)
Arch inclination angle α (deg.)	8 6-10 (23)	8 6-10 (21)	8 5-9 (29)
Transversal angle β (deg.)	152 145-161 (5)	152 145-160 (5)	152 146-162 (5)

N = 500 patients.
Data are median and interquartiles Q1 − Q3 (25th and 75th percentiles).
*$P < 0.01$, **$P < 0.001$ (Wilcoxon test with respect to men).
CQV% indicates coefficient of quartile variation calculated as $(Q3-Q1)/(Q1+Q3)\times 100$.

The scree plot (Fig. 3) shows 3 principal factors representing 46%, 22%, and 12% of the total variance with corresponding eigenvalues of 5.5, 2.7, and 1.5, respectively. The remaining eigenvalues were < 1. In other words, 80% of the variability in TA morphology inherent in the measured geometric parameters was explained with these 3 factors.

For the whole population, the aortic shape as a function of variation in the 3 principal factors (within the intervals of Eq. 1) is plotted in Figure 4 for the coronal plane. At first sight, factor 1 can be associated with a proportional size change (scale factor), factor 2 with an unfolding effect that can also be observed in the sagittal plane (Fig. 5), and factor 3 with a modification of the vessel symmetry. Animations are available as a supplementary material to better understand these variations (Videos F1, F2, and F3, Supplemental Digital Contents 1, 2, and 3, http://links.lww.com/JTI/A48, http://links.lww.com/JTI/A49, http://links.lww.com/JTI/A50). Further, centerline coordinates, normal vectors, and diameters for each reconstruction in Figure 4 are provided in an attached spreadsheet (Supplementary Table Average Aortas, Supplemental Digital Content 4, http://links.lww.com/JTI/A51).

The correlation of each geometric parameter with the 3 principal components can be observed in Figure 6. The parameters inside the dark gray band (strong correlation values, $|r| > 0.6$) and the light gray band (mild correlation, $0.6 > |r| > 0.4$) were analyzed for each factor. Factor 1 is dominated by a consistent increase of the principal size parameters (scale effect). In factor 2, arch width and height show an opposite behavior, and whereas arch tortuosity and inclination angle α increase, the transversal angle β decreases (unfolding effect). In factor 3, we observe that the inclination angle is reduced, and, whereas vector C_{45} shortens, the difference with vector C_{135} ($\Delta C = C_{135}-C_{45}$) grows (symmetry effect). To analyze whether the modes of variation were influenced by age, BSA, and 10-year FRS, the population was split into groups on the basis of median values that gave results of 58 years, 2.0 m^2, and 9.4%, respectively. The overall trend of the correlation values was similar in these subgroups with respect to the whole population (Fig. 6, where dashed lines represent the maximum and minimum correlation values found among all subgroups). Correlation coefficients for women were analyzed separately for each factor (dotted lines in Fig. 6). Curves followed the global trend, although some discrepancies in shape unfolding and symmetry factors (2 and 3) were observed (arrows in Fig. 6 indicate values that entered or left both significant correlation bands).

DISCUSSION

In this study, the anatomic variability of the human TA was analyzed in a cohort comprising 500 asymptomatic patients using extended noncontrast MSCT coronary scans that included the top of the aortic arch. PCA, applied to meaningful geometric parameters selected to describe the vessel tridimensional morphology, revealed that TA geometric variation can be successfully explained using 3 key factors that account for ~80% of the total variability

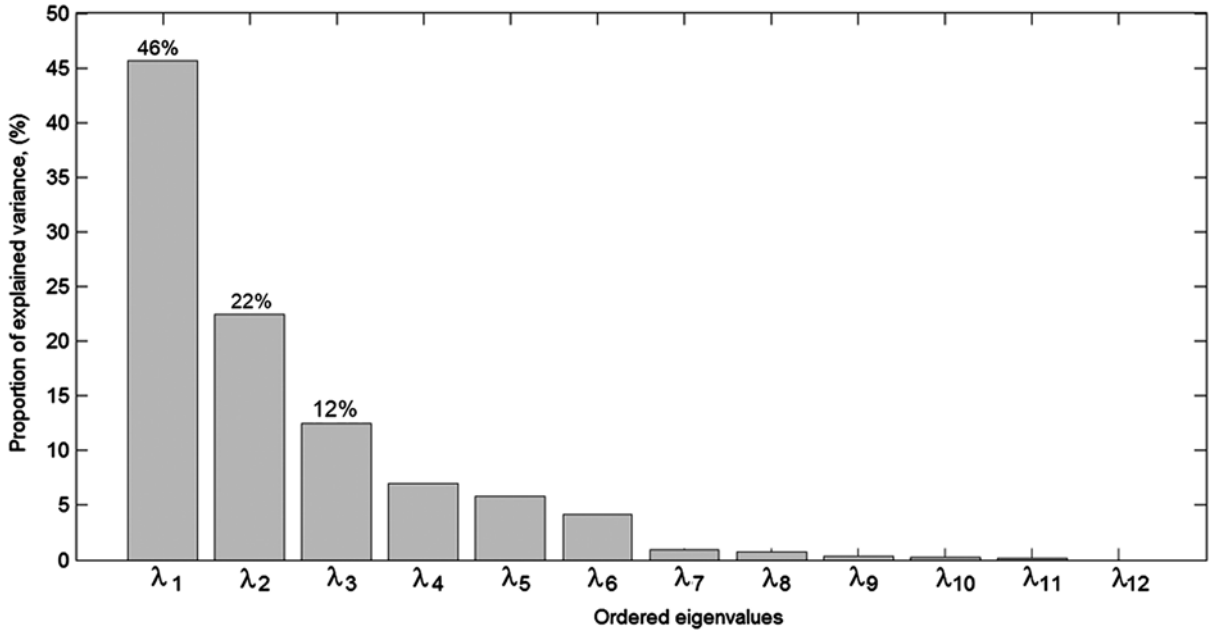

FIGURE 3. Scree plot representing the percentage of total variation for each eigenvalue of the covariance matrix, sorted in descending order. The first 3 factors account for 46%, 22%, and 12% of total variability, respectively.

expressed by these parameters. After analyzing the factor correlations and mean aortic shapes, each mode of variation showed a simple anatomic interpretation. The following dominant contributors resulted: (i) vessel size, (ii) arch unfolding, and (iii) arch symmetry, stating the basis for characterizing the variability of TA morphology. A spreadsheet with numerical data of averaged aortas, including centerline coordinates, normal vectors, and the corresponding diameter values are provided as supplementary material (Supplementary Table Average Aortas, Supplemental Digital Content 4, http://links.lww.com/JTI/A51). This quantitative information catalogues the aortic geometric variability of midlevel-risk patients and can be exploited by researchers interested in aortic blood flow simulations and stent-graft design.

The PCA in this study was applied to geometric parameters selected to describe TA size and shape characteristics (Fig. 2). A similar approach was successfully used to catalogue the geometry of the human coronary arteries.[16] Briefly, instead of estimating the vessel centerline coordinates to examine the statistics of the positions of the points in a classical point distribution model,[23] the variation of 12 anatomic variables that defined the vessel geometry were studied. Actually, the set of parameters was

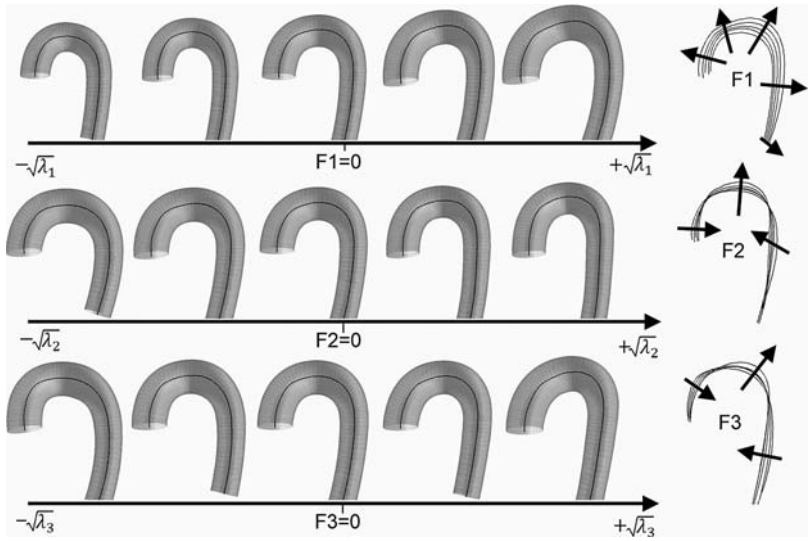

FIGURE 4. Averaged aortic shapes grouped in 5 intervals for positive and negative changes of each factor (Eq. 1). On the right, sketches of the observed effects produced by the increase of each factor over the aortic centerline are shown with arrows.

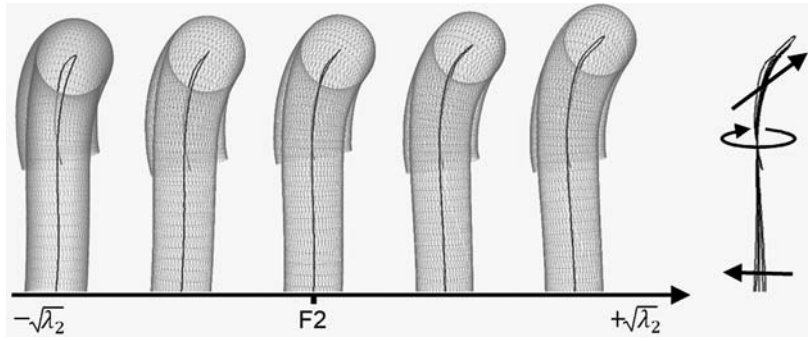

FIGURE 5. Lateral view of averaged aortic shapes for factor 2 (F_2). Positive and negative changes of F_2 are shown in 5 intervals. On the right, a sketch of the twisting effects produced by F_2 on aortic centerline.

not arbitrarily chosen. Recent reports on the aging influence on aortic diameter, length, arch width and height, radius of curvature, and tortuosity were determinant to define it.[22,24] Clinically, all these measures are easily interpreted by a radiologist. Further, our approach did not require any manual scaling/aligning process that could interfere with the variability assessment.[23] Vessels were segmented in 3D from noncontrast MSCT images, and all geometric parameters were measured from skeleton coordinates and their corresponding cross-section diameters using an aortic model. For each patient, inclination and transversal angles were referenced to their own regression plane to avoid aligning ambiguities (Fig. 2). Aortas were aligned using these planes and vectors connecting points CA and CD (Figs. 4, 5) only for visualization purposes and to better understand the different anatomic variations associated with each factor. Essentially, we proposed to explain the anatomic nature of geometric variability identifying those features with high loadings in the factor analysis and interpreting the variations.

The analysis of the geometric parameters exhibited a global moderate dispersion that did not exceed 23% (Table 2), showing that aortas conform to a singular morphology even for a heterogenous group of subjects. Variability of arch symmetry was particularly high due to negative values in the vector differences. In a sex comparison, aortas of women were proportionally smaller compared with those of men, although shape deformation parameters and dispersion values were similar (Table 2). To better summarize these variations by a smaller number of independent factors, a PCA was performed revealing 3 principal factors (scree plot in Fig. 3).

The first factor (F_1) was strongly associated with aortic size parameters: TA volume, length, mean diameter, arch width and height, and C_{45} and C_{135} vectors (top panel of Fig. 6, measures inside shaded region). As seen in Figure 4 and Video F1 (Supplemental Digital Content 1, http://links.lww.com/JTI/A48), all size parameters increase homogenously with F_1 (in the same direction). We can call F_1 a "scale factor" because of its overall relation to vessel size and because it is independent from shape parameters. In other words, 46% of total geometric variability in human TA can be attributed to a proportional size change. The correlation coefficients for women (dotted line in Fig. 6) followed the overall population curves, indicating that even with smaller vessels their mode of variation was similar.

The second factor (F_2) was positively associated with arch tortuosity, arch height, and inclination angle but negatively with arch width and transversal angle (Fig. 6). As seen in Figure 4 and Video F2 (Supplemental Digital Content 2, http://links.lww.com/JTI/A49), the increase of F_2 results in tall and narrow aortas that tend to bend in the sagittal plane. See how the inclination and transversal angles diminish for smaller values of F_2 in the lateral view of Figure 5. The inverse relation between aortic arch width and height in Figure 6 suggests that F_2 describes an anatomic variation associated with an uncoiling deformation of the aortic arch that simultaneously increases the vessel tortuosity. Consequently, we designated F_2 as an "unfolding factor," accounting for 22% of total variability. Aortic unfolding was shown as the consequence of a complex mechanism of aortic dilation and lengthening with aging, accelerated by hypertension.[22,25–27] In other reports, aortas were classified into 3 characteristic shapes related to arch morphology: circular or "romanesque," "gothic," and cubic or "crenel."[14,18] In 62 patients without TA disease, Frydrychowicz et al[14] found 11% of cubic, 71% circular, and 18% gothic arcs. A qualitative comparison of the average shapes found in this study using PCA suggests that the cubic form resembles the aortas with a low value of F_2 ($F_2 < \mu_2 - \sqrt{\lambda_2}$), aortas become circular for intermediate values (between $\mu_2 - \sqrt{\lambda_2}$ and $\mu_2 + \sqrt{\lambda_2}$), and tend to a Gothic shape for high values of this factor ($F_2 > \mu_2 + \sqrt{\lambda_2}$). Patients found in each of these intervals correspond to approximately 14%, 68%, and 17%, respectively, showing a similar proportion to that found in Frydrychowicz et al.[14] It should be noticed that these shapes emerged from mean aortas after PCA, without performing an explicit search for these particular geometries, suggesting that these shapes are also inherently related to the parameters studied in this work. Finally, a particular twisting over the regression plane can be observed in the lateral plane of Figure 5 as the aortic arch flattens. This effect is coherent with a decreased helicity or even a change in helix direction reported in older subjects.[14] Helical flow plays an important role in LDL transport and is thought to compensate the adverse effects of aortic curvature by protecting the arterial wall from atherogenic effects.[13] The morphologic variability described by F_2 seems to anatomically influence the aortic velocity profiles, arterial blood pressure,[28] and aortic stiffness[18,29] and could be a valid starting point to analyze helical flow patterns. In women, a similar unfolding behavior was observed, whereas it also involved a proximal descending

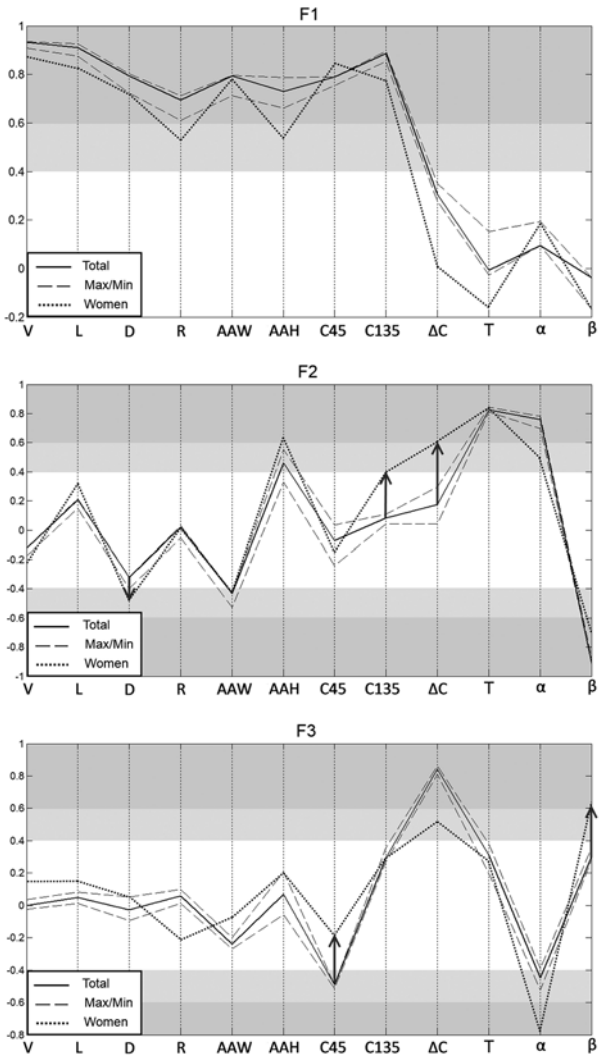

FIGURE 6. Coefficients of correlation (r) of each aortic geometric parameter in PCA for the 3 principal factors. Dark gray bands indicate strong correlations ($|r|>0.6$), and light gray bands indicate mild correlation ($0.6>|r|>0.4$). α and β indicate inclination and transversal angles; AAW and AAH, aortic arch width and height; C_{45} and C_{135}, arch vector distances, D, diameter; R, radius of curvature; L, length; T, tortuosity; V, volume. See Figure 2 for the definition of geometric parameters. Solid lines represent the r values obtained in the PCA of the entire population. Dashed lines represent the maximum and minimum r values found when the population was divided by medians of age, BSA, or FRS. Correlation values for women are shown with a dotted line, and arrows were included where r values differed from the entire population, entering or leaving the gray bands.

aorta deformation (C_{135}) that increased the correlation with the symmetric indicator ΔC (arrows in Fig. 6). This might indicate a specific asymmetric unfolding in women that deserves further attention in future works.

The third factor (F_3), which accounted for 12% of total variability, was dominated by this symmetrical parameter ΔC, defined as the difference between C_{45} and C_{135} vectors. When F_3 grows, ΔC increases and C_{45} decreases (bottom panel of Fig. 6). This particular effect, which pushes the ascending portion toward the center while pulling the proximal descending segment, can be perceived from the sketch in the bottom right corner of Figure 4 and Video F3 (Supplemental Digital Content 3, http://links.lww.com/JTI/A50). Accordingly, F_3 was designated as the "symmetry factor," representing the skew deformation of the aortic arch. In women, we observed that these deformations were slightly attenuated with a more pronounced influence of the transversal and inclination angles (Fig. 6). A numerical simulation as in Liu et al[13] is being designed to provide new insights on the specific role of F_3 on aortic flow and velocity profiles.

In the present study, the role of age, BSA, and FRS on TA morphology variability was also assessed. Maximum and minimum correlation coefficients can be observed with dashed lines in Figure 6. Globally, all relevant parameters presented a negligible deviation. This should not lead to the misinterpretation that TA mean geometric parameters are independent from aging, body size, or the patient risk profile. The fact that the correlation coefficients between these parameters and the 3 main factors remained stable indicates that there exist a natural variability of TA geometry that is not modified by age, BSA, or FRS. Although a "standard aortic arch" does not really exist[4] due to the complex 3D structure of the aorta, the anatomic variability can still be quantified using the proposed method.

Some limitations of the present study need to be addressed. Inherent to the nature of noncontrast MSCT images, only external diameters were measured during a static phase of the cardiac cycle. The assessment of arterial wall thickness and time dependencies would require other techniques such as enhanced CT or magnetic resonance imaging.[22] We decided to exploit coronary calcium scans, extending the FOV by 15% to cover the top of the aortic arch. Radiation exposure for the patient always remained <2 mSv. Regarding the segmentation algorithm, the proposed model required some manual interventions with an estimated intraobserver coefficient of variation of $<4\%$.[3] The circular shape assumption was efficient to extract the vessel centerline and to estimate a diameter, even in the presence of calcified lesions and supra-aortic branches. The inclusion of data regarding the configuration of these branches would have been beneficial but would have also required additional user interventions. Regarding the anatomic landmarks, the aortic root was excluded, and the ascending aorta was defined starting at the ostium of left coronary artery. As the aortic annulus has an oval shape,[30] the circular assumption in the current model should be revised to include it in the proximal ascending portion. Distally, a cross-sectional circularity was actually observed in our population. It is noteworthy that diameter measures are still widely informed using traditional methods (eg, angiography). Moreover, using a circle rather than an arbitrary contour shape was effective for the reconstruction of average vessels, as circles lying in an equivalent centerline position were straightforwardly compared between subjects and needed no angular alignment. Still, other methods recently reported using a level set framework could be explored to improve the cross-sectional shape assessment and to reduce reading variability.[31] Substantially more men than women were included in this study because of a bias in subjects referred to cardiovascular tests by general practitioners to our hospital. Finally, only midlevel-risk patients with no abnormal aortas were selected for this study. Modifications in the segmentation algorithm should be introduced in future studies to assess the morphology variation in diseased aortas.

In conclusion, noncontrast MSCT scans allowed the reconstruction, modeling, and meshing of the entire TA, offering new valuable extracoronary information with respect to the original goal of calcium score assessment. A PCA carried out on aortic morphology showed that vessel size, arch unfolding, and arch symmetry are the principal modes of anatomic variation, accounting for 46%, 22%, and 12% of total variability, respectively. Age, body size, and risk factors did not modify this distribution. The morphometric information reported in this study is aimed at constructing a quantitative catalog of average TAs in midlevel-risk patients.

REFERENCES

1. Greenland P, Alpert JS, Beller GA, et al. 2010 ACCF/AHA Guideline for assessment of cardiovascular risk in asymptomatic adults: a report of the American College of Cardiology Foundation/American Heart Association Task Force on practice guidelines developed in collaboration with the American Society of Echocardiography, American Society of Nuclear Cardiology, Society of Atherosclerosis Imaging and Prevention, Society for Cardiovascular Angiography and Interventions, Society of Cardiovascular Computed Tomography, and Society for Cardiovascular Magnetic Resonance. *J Am Coll Cardiol*. 2010;56:e50–e103.
2. Wong ND, Gransar H, Shaw L, et al. Thoracic aortic calcium versus coronary artery calcium for the prediction of coronary heart disease and cardiovascular disease events. *JACC Cardiovasc Imaging*. 2009;2:319–326.
3. Craiem D, Chironi G, Redheuil A, et al. Aging impact on thoracic aorta 3D morphometry in intermediate-risk subjects: looking beyond coronary arteries with non-contrast cardiac CT. *Ann Biomed Eng*. 2012;40:1028–1038.
4. Demertzis S, Hurni S, Stalder M, et al. Aortic arch morphometry in living humans. *J Anat*. 2010;217:588–596.
5. Elefteriades JA, Farkas EA. Thoracic aortic aneurysm clinically pertinent controversies and uncertainties. *J Am Coll Cardiol*. 2010;55:841–857.
6. Hiratzka LF, Bakris GL, Beckman JA, et al. 2010 ACCF/AHA/AATS/ACR/ASA/SCA/SCAI/SIR/STS/SVM Guidelines for the diagnosis and management of patients with thoracic aortic disease. A report of the American College of Cardiology Foundation/American Heart Association Task Force on Practice Guidelines, American Association for Thoracic Surgery, American College of Radiology, American Stroke Association, Society of Cardiovascular Anesthesiologists, Society for Cardiovascular Angiography and Interventions, Society of Interventional Radiology, Society of Thoracic Surgeons, and Society for Vascular Medicine. *J Am Coll Cardiol*. 2010;55:e27–e129.
7. Rousseau H, Chabbert V, Maracher MA, et al. The importance of imaging assessment before endovascular repair of thoracic aorta. *Eur J Vasc Endovasc Surg*. 2009;38:408–421.
8. Worz S, von Tengg-Kobligk H, Henninger V, et al. 3-D quantification of the aortic arch morphology in 3-D CTA data for endovascular aortic repair. *IEEE Trans Biomed Eng*. 2010;57:2359–2368.
9. Gyongyosi M, Yang P, Khorsand A, et al. Longitudinal straightening effect of stents is an additional predictor for major adverse cardiac events. Austrian Wiktor Stent Study Group and European Paragon Stent Investigators. *J Am Coll Cardiol*. 2000;35:1580–1589.
10. Brozzi NA, Roselli EE. Endovascular therapy for thoracic aortic aneurysms: state of the art in 2012. *Curr Treat Options Cardiovasc Med*. 2012;14:149–163.
11. Monahan TS, Schneider DB. Fenestrated and branched stent grafts for repair of complex aortic aneurysms. *Semin Vasc Surg*. 2009;22:132–139.
12. Ueda T, Fleischmann D, Rubin GD, et al. Imaging of the thoracic aorta before and after stent-graft repair of aneurysms and dissections. *Semin Thorac Cardiovasc Surg*. 2008;20:348–357.
13. Liu X, Pu F, Fan Y, et al. A numerical study on the flow of blood and the transport of LDL in the human aorta: the physiological significance of the helical flow in the aortic arch. *Am J Physiol Heart Circ Physiol*. 2009;297:H163–H170.
14. Frydrychowicz A, Berger A, Munoz Del Rio A, et al. Interdependencies of aortic arch secondary flow patterns, geometry, and age analysed by 4-dimensional phase contrast magnetic resonance imaging at 3 Tesla. *Eur Radiol*. 2012;22:1122–1130.
15. Malek AM, Alper SL, Izumo S. Hemodynamic shear stress and its role in atherosclerosis. *JAMA*. 1999;282:2035–2042.
16. Zhu H, Ding Z, Piana RN, et al. Cataloguing the geometry of the human coronary arteries: a potential tool for predicting risk of coronary artery disease. *Int J Cardiol*. 2009;135:43–52.
17. Bryan R, Mohan PS, Hopkins A, et al. Statistical modelling of the whole human femur incorporating geometric and material properties. *Med Eng Phys*. 2010;32:57–65.
18. Ou P, Celermajer DS, Mousseaux E, et al. Vascular remodeling after "successful" repair of coarctation: impact of aortic arch geometry. *J Am Coll Cardiol*. 2007;49:883–890.
19. Greenland P, Alpert JS, Beller GA, et al. 2010 ACCF/AHA guideline for assessment of cardiovascular risk in asymptomatic adults: a report of the American College of Cardiology Foundation/American Heart Association Task Force on Practice Guidelines. *Circulation*. 2010;122:e584–e636.
20. Chironi G, Orobinskaia L, Megnien JL, et al. Early thoracic aorta enlargement in asymptomatic individuals at risk for cardiovascular disease: determinant factors and clinical implication. *J Hypertens*. 2010;28:2134–2138.
21. Hotelling H. Analysis of a complex of statistical variables into principal components. *J Educ Psychol*. 1933;24:417–441.
22. Redheuil A, Yu WC, Mousseaux E, et al. Age-related changes in aortic arch geometry: relationship with proximal aortic function and left ventricular mass and remodeling. *J Am Coll Cardiol*. 2011;58:1262–1270.
23. Cootes TF, Taylor CJ, Cooper DH, et al. Active shape models—their training and application. *Comput Vis Image Underst*. 1995;61:38–59.
24. Craiem D, Casciaro ME, Graf S, et al. Effects of aging on thoracic aorta size and shape: a non-contrast CT study. Engineering in Medicine and Biology Society (EMBC), 2012 Annual International Conference of the IEEE, San Diego, USA. August 28, San Diego, USA. August 28, 2012:4986–4989.
25. Craiem D, Chironi G, Casciaro ME, et al. Three-dimensional evaluation of thoracic aorta enlargement and unfolding in hypertensive men using non-contrast computed tomography. *J Hum Hypertens*. 2013;27:504–509.
26. O'Rourke M, Farnsworth A, O'Rourke J. Aortic dimensions and stiffness in normal adults. *JACC Cardiovasc Imaging*. 2008;1:749–751.
27. Sugawara J, Hayashi K, Yokoi T, et al. Age-associated elongation of the ascending aorta in adults. *JACC Cardiovasc Imaging*. 2008;1:739–748.
28. Ou P, Bonnet D, Auriacombe L, et al. Late systemic hypertension and aortic arch geometry after successful repair of coarctation of the aorta. *Eur Heart J*. 2004;25:1853–1859.
29. Ou P, Celermajer DS, Raisky O, et al. Angular (Gothic) aortic arch leads to enhanced systolic wave reflection, central aortic stiffness, and increased left ventricular mass late after aortic coarctation repair: evaluation with magnetic resonance flow mapping. *J Thorac Cardiovasc Surg*. 2008;135:62–68.
30. Tops LF, Wood DA, Delgado V, et al. Noninvasive evaluation of the aortic root with multislice computed tomography implications for transcatheter aortic valve replacement. *JACC Cardiovasc Imaging*. 2008;1:321–330.
31. Kurugol S, San Jose Estepar R, Ross J, et al. Aorta segmentation with a 3D level set approach and quantification of aortic calcifications in non-contrast chest CT. Engineering in Medicine and Biology Society (EMBC), 2012 Annual International Conference of the IEEE, San Diego, USA. August 28, 2012:2343–2346.